https://doi.org/10.5194/egusphere-2026-857
Preprint. Discussion started: 27 February 2026

Continuous analysis of N_2O isotopic composition during biological nitrogen removal in wastewater treatment to disentangle production and reduction processes

Hannes Keck[1], Laurence Strubbe[2,3], Paul M. Magyar[1], Adriano Joss[2], Andreas Froemelt[2], André Kupferschmid[4], Klaus-Holger Knorr[5] and Joachim Mohn[1]

[1]Empa, Laboratory for Air Pollution / Environmental Technology, Dübendorf, 8600, Switzerland
[2]Eawag, Swiss Federal Institute of Aquatic Science and Technology, Überlandstrasse 133, 8600, Dübendorf, Switzerland
[3]Vito, Flemish Institute for Technological Research, Mol, 2400, Belgium
[4]Empa, Transport at Nanoscale Interfaces, Dübendorf, 8600, Switzerland
[5]Institute of Landscape Ecology, Ecohydrology & Biogeochemistry Group, University of Münster, Münster, 48149, Germany

Correspondence to: Hannes Keck (hannes.keck@empa.ch)

Abstract. Nitrous oxide (N_2O) is a potent greenhouse gas, and emissions from wastewater treatment plants (WWTPs) represent a significant and highly variable source. Understanding the dynamics in microbial pathways of N_2O formation and reduction during biological nitrogen removal is essential for targeted mitigation strategies. Stable isotope analysis of N_2O ($\delta^{15}N^{\alpha}$, $\delta^{15}N^{\beta}$, $\delta^{18}O$, and ^{15}N site preference) provides a powerful tool to disentangle and quantify N_2O production and reduction processes, yet conventional analytical approaches lack temporal resolution. Here, we present the first long-term application of an off-axis integrated cavity output spectrometer for real-time N_2O isotopic analysis at a pilot-scale WWTP over one year of operation. We developed a dynamic dilution system and implemented correction protocols for drift, N_2O mole fraction dependence, and gas matrix effects on isotopic results, achieving uncertainties of 0.85 ‰ ($\delta^{15}N^{\alpha}$), 1.08 ‰ ($\delta^{15}N^{\beta}$), 0.81 ‰ ($\delta^{15}N^{bulk}$), 0.48 ‰ ($\delta^{18}O$) and 1.09 ‰ (^{15}N site preference). Representative datasets demonstrate the system's capability to (i) identify dominant N_2O production pathways under standard operation, (ii) quantify N_2O reduction in relation to dissolved oxygen concentration, and (iii) trace nitrogen transformation during low-level ^{15}N-labelling experiments. Our results indicate nitrifier or heterotrophic denitrification as the main source of N_2O, and that N_2O reduction efficiency is strongly controlled by oxygen availability. This study highlights the potential of laser spectroscopy for continuous isotopic monitoring in real-world engineered systems and provides practical guidelines for uncertainty reduction and data interpretation. More specifically, our work forms a foundation for further investigations of the operational factors controlling N_2O formation and N_2O reduction in biological WWTPs and other complex anthropogenically-perturbed settings.

https://doi.org/10.5194/egusphere-2026-857
Preprint. Discussion started: 27 February 2026

1. Introduction

Nitrous oxide is one of the most important greenhouse gases in the atmosphere, with a 100-year global warming potential of 273 CO_2 equivalents and a relative contribution to the total radiative forcing of about 6 % (IPCC, 2021). Anthropogenic activities enhance N_2O emissions, outweighing stratospheric destruction and leading to an increase in atmospheric N_2O concentrations from 1750 to 2022 by about 25 % with an annual growth rate currently exceeding 1 ppb yr^{-1} (WMO, 2024). On a global scale the largest share of man-made emissions is attributed to the agricultural sector, followed by fossil fuel combustion and industrial processes (Tian et al., 2024). N_2O emissions from wastewater treatment plants (WWTP) have long been underestimated, but long-term full-scale monitoring data have provided evidence for higher and more variable emission factors than had previously been assumed (Daelman et al., 2015; Gruber et al., 2021; Kosonen et al., 2016). As N_2O emission monitoring is not part of normal operation control at WWTPs, countries still rely on using emission factors for their reporting. Emission factors for N_2O from wastewater treatment were adjusted to 1.6 % of the total nitrogen load, as compared to a previously applied value as low as 0.035 % (EEA, 2017; IPCC, 2019). But different emission factors are still implemented for reporting in European countries (EEA, 2023). Moreover, emissions were found to be related to plant operation (Gruber et al., 2021), and intermittency controlled by problematic situations, such as hampered microbial conversion or addition of supernatant from anaerobic digestion (Froemelt et al., 2025; Gruber et al., 2021). Applying a country-specific approach, Switzerland's National Greenhouse Gas Inventory reports wastewater treatment as the second largest source of N_2O accounting for about 20 % of national N_2O emissions, only topped by agriculture (BAFU, 2025). Consequently, the relevance of WWTPs as N_2O emission point-sources and their controlled operation makes them attractive targets for N_2O emission mitigation.

Nitrous oxide from WWTPs mainly originates from the biological nitrogen removal process (Kampschreur et al., 2009). In a conventional biological nitrogen removal process, N_2O is primarily produced by three microbial pathways mediated by two bacterial groups. Bacterial ammonium oxidizers emit N_2O during two processes, namely hydroxylamine oxidation (Hy) and nitrifier denitrification (nD). Hydroxylamine oxidation forms N_2O as a side product during NH_4^+ oxidation to NO_2^-. Nitrifier denitrification reduces NO_2^- to N_2O with NH_4^+ as the electron donor. The second bacterial group, the ordinary heterotrophic organisms, couple oxidation of organic substrates to reduction of NO_3^-, NO_2^-, NO, and N_2O in heterotrophic denitrification (hD). During hD NO and N_2O can be emitted as obligatory intermediates. However, hD can also act as a N_2O sink process, reducing N_2O to N_2. The relative contributions and interactions of these pathways in a process workflow with variable control parameters and substrate availability remain poorly understood (Law et al., 2012). A comprehensive assessment of the active biological processes and their interplay is crucial for a targeted control and optimization of reactor and process design to minimize N_2O emissions, while maintaining efficient nitrogen removal.

Analyzing the stable isotopic composition ($^{15}N/^{14}N$, $^{18}O/^{16}O$) of the asymmetric N_2O molecule has proven to be powerful tool to disentangle N_2O production pathways and to quantify the extent of N_2O reduction to N_2 in laboratory and full-scale WWTP settings (Gruber et al., 2022; Harris et al., 2015; Tumendelger et al., 2016; Wunderlin et al., 2013). The relative

https://doi.org/10.5194/egusphere-2026-857
Preprint. Discussion started: 27 February 2026

abundances of the rare N_2O isotopologues $^{14}N^{15}N^{16}O$ (^{15}N in the central, α position), $^{15}N^{14}N^{16}O$ (^{15}N in the terminal, β position), and $^{14}N^{14}N^{18}O$, relative to the main isotopic species ($^{14}N^{14}N^{16}O$) in a sample are expressed relative to standards (air-N_2 for $^{15}N/^{14}N$, VSMOW for $^{18}O/^{16}O$) in the δ-notation (Camin et al., 2025; Toyoda and Yoshida, 1999). Transformations during metabolic pathways (i.e. Hy, hD and nD) are associated with kinetic or equilibrium fractionation processes and leave their imprint on the isotopic composition of the emitted N_2O (Toyoda et al., 2015). An important characteristic of a N_2O formation process is the difference in ^{15}N substitution in central and terminal position, named site preference (SP = $\delta^{15}N^{\alpha}$ - $\delta^{15}N^{\beta}$), which is mainly controlled by the N-N bond formation (Toyoda et al., 2015). Data are often presented in a dual isotopic plot of SP versus $\delta^{18}O$ or SP versus $\delta^{15}N^{bulk}$ ($\delta^{15}N^{bulk}$ = ($\delta^{15}N^{\alpha}$ + $\delta^{15}N^{\beta}$) / 2) and compared to isotopic signatures retrieved from pure culture studies to aid the identification of N_2O source processes (Yu et al., 2020). Furthermore, during N_2O reduction to N_2 by hD, N_2O molecules in which ^{14}N is bound to ^{16}O are preferentially reduced, leading to an enhancement in $\delta^{15}N^{bulk}$, SP, and $\delta^{18}O$ in the remaining N_2O pool (Lewicka-Szczebak et al., 2017; Ostrom et al., 2007). This observation can be exploited to calculate the residual fraction of N_2O ($resN_2O$), if the isotopic signature of the initial unaffected N_2O pool for either $\delta^{15}N^{bulk}$, SP, or $\delta^{18}O$ (i.e. δ_0) is known and the corresponding composition of the remaining N_2O fraction (δ_R) is measured (Lewicka-Szczebak et al., 2017; Mariotti et al., 1981; Ostrom et al., 2007):

$$\delta_R - \delta_0 = \varepsilon \ln resN_2O \quad (1)$$

This calculation utilizes literature estimates for ε, the enrichment factor for N_2O reduction, here defined so that a negative value corresponds to a normal isotope effect, i.e. the light isotope reacts faster than the heavier one (Yu et al., 2020; Ostrom et al. 2007). The fraction of reduced N_2O (redN2O), i.e. the fraction of formed N_2, can be calculated by redN2O = 1 – $resN_2O$.

To date, however, most N_2O isotope studies, whether using natural isotopic abundance or ^{15}N or ^{18}O-labelling, have quantified N_2O reduction using bag sampling and subsequent laboratory analysis, which is labour intensive and offers only limited temporal resolution, incapable of tracing process changes at timescales relevant for WWTPs that exhibit strong daily as well as seasonal dynamics (Domingo-Félez et al., 2024; Gruber et al., 2020).

Laser spectroscopy offers the potential for continuous data on the isotopic composition of greenhouse gases, but apparent δ-values are dependent on the composition of the analyte gas and need correction schemes to produce accurate data (e.g. Sperlich et al., 2024). This is particularly important for process studies with strong changes in the concentrations of the target species, interfering trace gases, and the bulk gas composition. In recent years, different optical detection schemes, such as direct absorption spectroscopy, cavity ring-down spectroscopy and off-axis integrated cavity output spectroscopy (OA-ICOS) have been implemented for analysis of N_2O isotopic composition (e.g. Harris et al., 2020). Analyser models from different manufacturers, including the OA-ICOS spectrometer model applied here, have been tested under laboratory settings (Harris et al., 2020) and the mathematical formalism for data processing has been implemented and validated (Havsteen et al., 2025). However, until now, very few long-term applications of laser spectroscopy for N_2O isotope analysis under field conditions have been realized.

https://doi.org/10.5194/egusphere-2026-857
Preprint. Discussion started: 27 February 2026

Here, we implemented and tested a laser spectroscopic platform capable of real-time analysis of N_2O concentrations and isotopic composition. We demonstrate first on-line measurements during aeration phases at a pilot-scale WWTP over one year of operation to illustrate its potential for process identification. More specifically, we present three representative data sets: the first originates from periods of standard reactor operation that will help us distinguishing between the N_2O production pathways of Hy and denitrification (nD and hD); the second aims at exploring the influence O_2 availability on the N_2O reduction dynamics; and the third to demonstrate the systems potential for N_2O isotope analysis in low-level ^{15}N labelling studies. We provide practical recommendation how to reduce contributions to uncertainty in δ-values from variable gas composition and give guidelines on data analysis and uncertainty assessment.

2. Methods

2.1 Laser spectroscopic platform

An OA-ICOS (N_2OIA-30e-EP, model 914-0027, serial number: 14-0283, ABB – Los Gatos Research Inc., USA) was used to analyse the abundance of gaseous N_2O and its isotopic composition ($\delta^{15}N^{\alpha}$, $\delta^{15}N^{\beta}$, $\delta^{18}O$). The analyser uses a quantum cascade laser emitting at 2192.1–2192.5 cm^{-1}, which covers the target species but also spectral lines of CO_2 and CH_4 (Harris et al., 2020). The analyser has a built-in sample pump which maintains the target pressure in the cavity (60.12 hPa) and a sample gas flow of about 200 mL min^{-1}. The analyser software displays the absorption signal and provides N_2O concentration and δ-values in real-time at maximum temporal resolution of one spectrum per second. Further information on the analytical platform is described in Baer et al. (2002).

2.2 Identify optimal measurement conditions for wastewater treatment

In this study we target real-time data analysis using a practical instrumental approach, which can be implemented at WWTPs. Analysing N_2O from the undiluted source process for source attribution, we aim at a maximum uncertainty of 1 ‰ for $\delta^{15}N^{\alpha}$, $\delta^{15}N^{\beta}$, $\delta^{15}N^{bulk}$, $\delta^{18}O$ and SP for final corrected δ-values. In the following sections optimal averaging times, drift correction and calibration approaches as well as uncertainty contributions from variable gas composition are evaluated. We followed the mathematical formalism and adapted the MATLAB algorithm provided by Havsteen et al. (2025).

2.2.1 Allan precision

In an initial test phase, important characteristics of the analyser performance were determined in accordance with Harris et al. (2020) to define a strategy for real-time measurements at WWTPs. Optimal averaging times to reach adequate precision levels (i.e. 0.2 ‰) and drift effects were determined using the Allan variance technique (Allan, 1966; Werle et al., 1993). For this, a gas mixture with known N_2O isotopic composition (Cal1, see Tab. 1) was dynamically diluted with N_2O-free synthetic air (SA, 78.1 % N_2, 20.96 (±0.4) % O_2, 0.95 (±0.02) % Ar, Carbagas AG, Switzerland) to a concentration of 12 ppm N_2O

https://doi.org/10.5194/egusphere-2026-857
Preprint. Discussion started: 27 February 2026

and a total flow of 300 mL min^{-1} and measurements were recorded for more than 3.5 days. The Allan precision for δ-values for 5- and 10-minutes integration time were 0.08 – 0.09 ‰ and 0.06 – 0.07 ‰, respectively (Fig. 1). Instrumental drifts over 24-hour periods were estimated on basis of the Allan analysis and accounted for 0.26 ‰, 0.36 ‰, 0.05 ‰, 0.40 ‰, and 0.85 ‰ for $\delta^{15}N^{\alpha}$, $\delta^{15}N^{\beta}$, $\delta^{15}N^{bulk}$, $\delta^{18}O$, and SP, respectively.

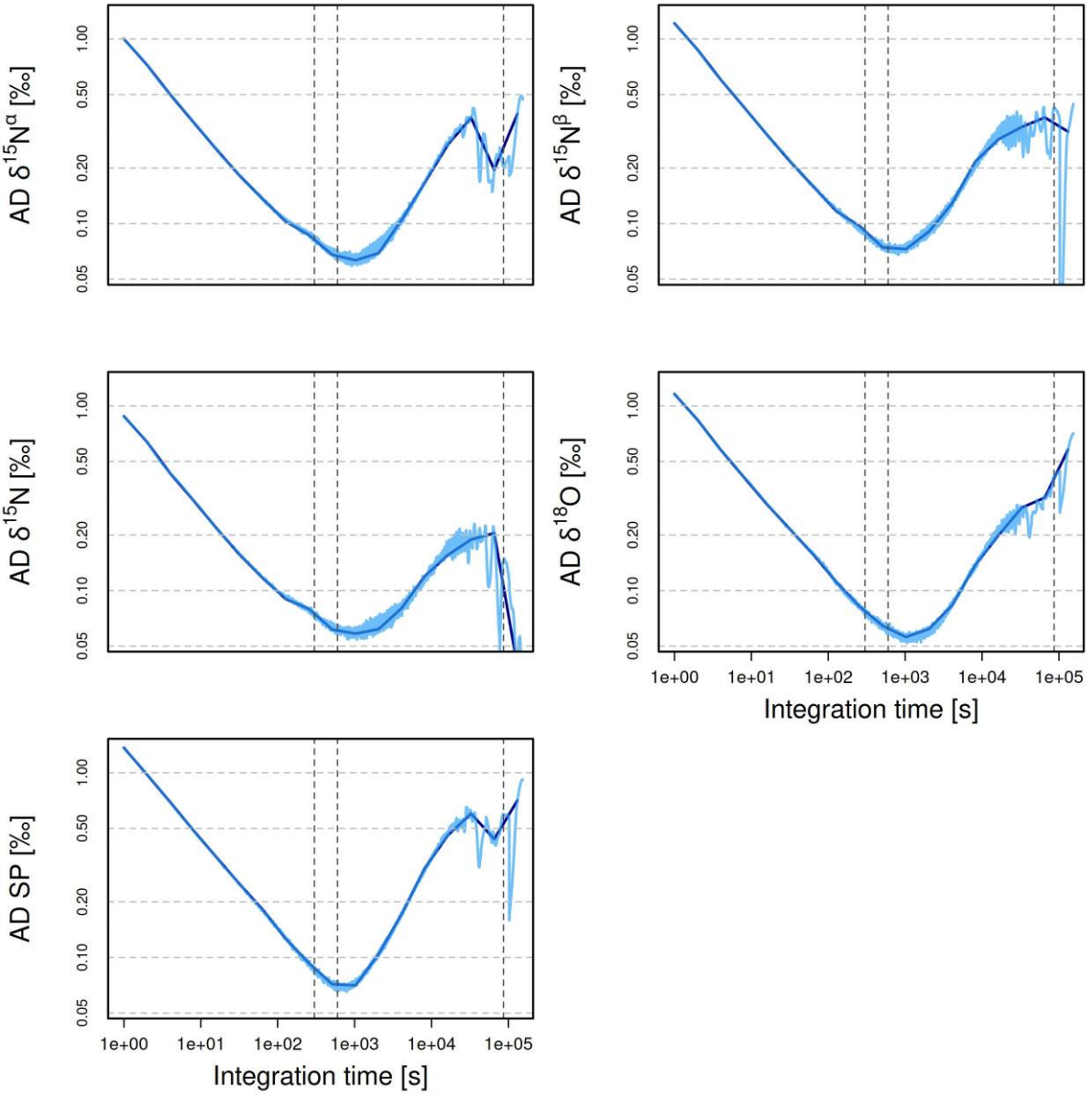

Figure 1: Allan deviations (AD), i.e. precision as function of integration time for $\delta^{15}N^{\alpha}$, $\delta^{15}N^{\beta}$, $\delta^{15}N^{bulk}$, $\delta^{18}O$, and SP measured by an OA-ICOS analyser at 12 ppm N_2O. Dashed vertical lines are placed at 5 and 10 minutes and at 24 hours integration time.

https://doi.org/10.5194/egusphere-2026-857
Preprint. Discussion started: 27 February 2026

2.2.2 Calibration procedure, drift correction and target gas measurements

From every measurement interval the first three to five minutes were discarded to assure complete exchange of the analyte gas and only the last 5 minutes were averaged before further data processing. To reduce drift effects and enable offset correction, every analyte gas measurement was bracketed by a calibration gas (Cal1, Tab. 1) measurement. A second calibration gas (Cal2, Tab. 1) was measured before and after each experiment or every eight hours during continuous measurements for two-point δ-calibration.

Table 1: N_2O concentration, isotopic composition and gas matrix of the calibration gases (Cal1, Cal2) and the target gas used in this study.

	N_2O [ppm]	$\delta^{15}N^{\alpha}$ [‰]	$\delta^{15}N^{\beta}$ [‰]	$\delta^{15}N^{bulk}$ [‰]	$\delta^{18}O$ [‰]	SP [‰]	Gas matrix[2)]
Cal1[1)]	98.3 (±1.9)	-0.74 (±0.19)	0.44 (±0.15)	-0.15 (±0.13)	38.74 (±0.23)	-1.2 (±0.23)	78.2 % N_2, 20.92 (±0.2) % O_2, 0.91 (±0.05) % Ar
Cal2[3)]	90.2[5)]	50.95 (±0.47)	55.09 (±0.47)	53.02 (±0.05)	103.04 (±0.16)	-4.13 (±0.93)	78.1 % N_2, 20.95 (±0.4) % O_2, 0.95 (±0.02) % Ar
Target gas[4)]	90.1[5)]	-24.35 (±0.32)	-22.94 (±0.33)	-23.64 (±0.03)	31.79 (±0.12)	-1.41 (±0.46)	79.5 % N_2, 20.5 % (±0.2) O_2

[1)] Commercial gas mixture, procured from Linde Gas AG (Switzerland), isotopic composition analysed by Empa. The precision indicated is the standard deviation for replicate sample measurements and does not include the uncertainties of the calibration chain.
[2)] Manufacturer's specifications.
[3)] Empa cylinder D689516; N_2O isotopic composition of pure N_2O gas reported in (Mohn et al., 2022); the gas matrix contains additional trace gases: 400 (±8) ppm CO_2, 2 (±0.2) ppm CH_4, 200 (±40) ppb CO (manufacturer's specifications). Differences in gas matrix composition, i.e. presence of trace gases (CO_2, CH_4, CO) in Cal2, given the applied strong dilution with high purity SA are not expected to affect analytical results (see Harris et al., 2020).
[4)] Empa cylinder CA06266; N_2O isotopic composition analysed by IRMS by Sakae Toyoda at Science Tokyo. The precision indicated is the standard deviation for replicate sample measurements and does not include the uncertainties of the calibration chain.
[5)] N_2O concentration estimated from N_2O and SA volume used for production.

Accuracy of measurements was assessed using target gas measurements (Tab. 1), performed in four blocks distributed over the complete measurement period (24th September 2024, 30th and 31st January 2025, 11th September 2025). Each measurement block consisted of four 10-minute analyses of the target gas and was performed in an identical manner as any experimental measurements, i.e. with two-point calibration before and after each target gas measurement block and bracketed with Cal1 measurements. Average results were -25.51 ± 0.31, -23.35 ± 0.89, -24.43 ± 0.49, 31.22 ± 0.21 and -2.15 ± 0.90 ‰ for $\delta^{15}N^{\alpha}$, $\delta^{15}N^{\beta}$, $\delta^{15}N^{bulk}$, $\delta^{18}O$ and SP, respectively. Consequently, OA-ICOS results were systematically (0.4 to 1.2 ‰) lower than delta values reported by IRMS (Tab. 1). This discrepancy was not further addressed as it is within the

https://doi.org/10.5194/egusphere-2026-857
Preprint. Discussion started: 27 February 2026

uncertainty targets of our study. It might be rationalized by the absence of argon in the target gas tank, which was shown to lead to lower apparent delta values for OA-ICOS (Harris et al., 2020).

2.2.3 Nitrous oxide mole fraction dependence

The analyser's dependence of reported δ-values on variations in N_2O concentration was assessed by dynamic dilution of a reference gas (Cal1) with N_2O free dilution air to a sequence of N_2O concentrations ranging from 0.5 to 90 ppm. Gas mixtures were prepared at a flow rate of 300 mL min^{-1} and measurements recoded for 10 minutes per concentration step. To account for analyser drift, in-between every concentration step the Cal1 gas was diluted to 12 ppm and measured as a reference point. This experiment was repeated three times on different days prior to the measurement period at the pilot reactors and once after the measurement period of 12 months. This enabled us to assess the analyser-specific variation in N_2O concentration dependence in the short and long term.

Figure 2 displays apparent δ-values for Cal1 measured between 0.5 and 90 ppm N_2O. In accordance with earlier work (Harris et al., 2020) the concentration dependence was strongest towards low, i.e. ambient, concentration values and less pronounced above 6 ppm N_2O. Only in a concentration range from 8 to 20 ppm N_2O could reported $\delta^{15}N^{\alpha}$ and $\delta^{15}N^{\beta}$ values be described by a quadratic function (Fig. 2). For $\delta^{18}O$ the concentration range for which a quadratic correction function applies was even smaller, 8 to 16 ppm N_2O. Like (Plouviez et al., 2026), we observed significant temporal changes in the N_2O non-linearity over time, necessitating a dynamic dilution as well as corrections for the non-linear mole fraction dependence (see section 2.4.1).

https://doi.org/10.5194/egusphere-2026-857
Preprint. Discussion started: 27 February 2026

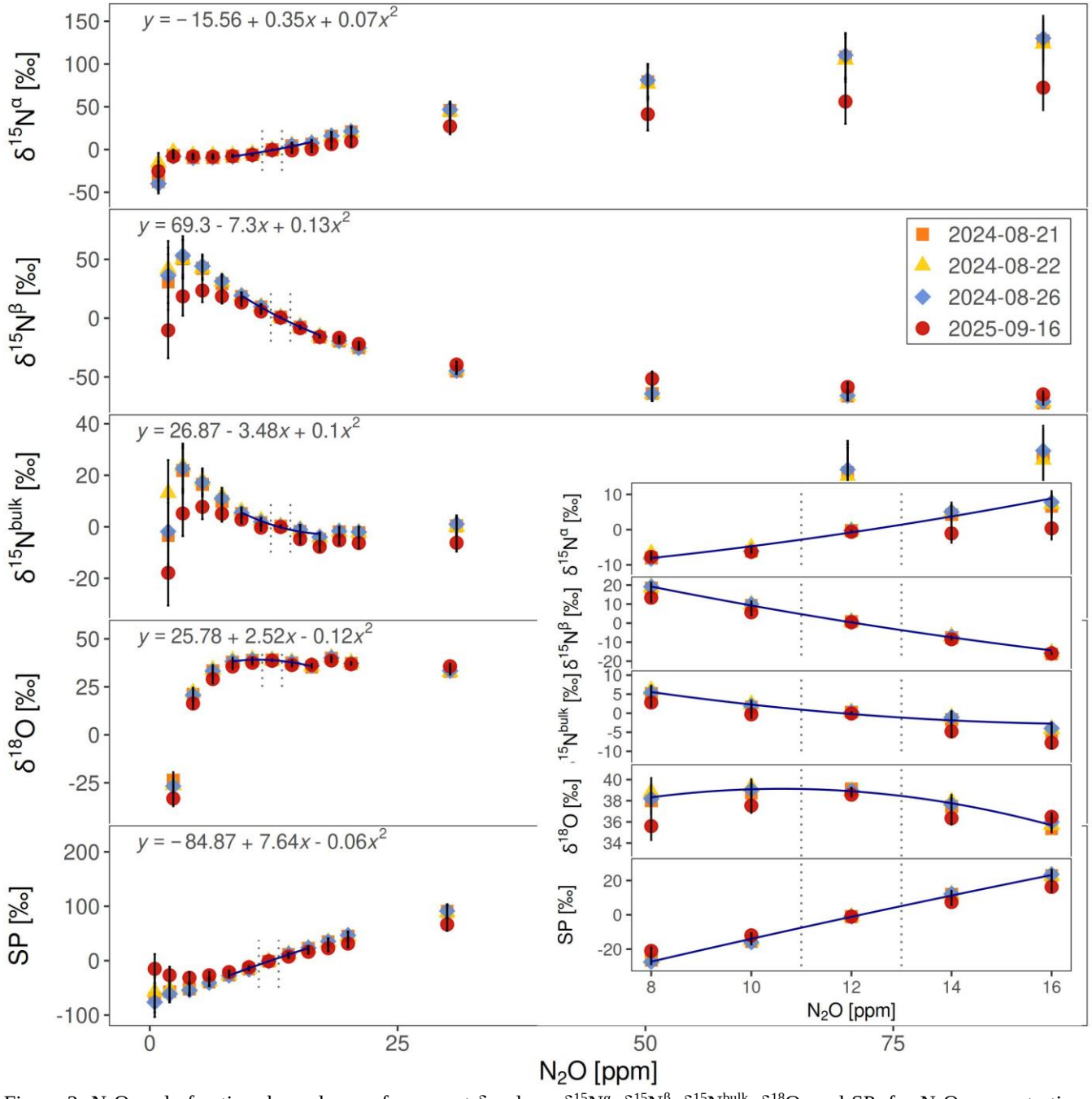

Figure 2: N_2O mole fraction dependence of apparent δ-values, $\delta^{15}N^{\alpha}$, $\delta^{15}N^{\beta}$, $\delta^{15}N^{bulk}$, $\delta^{18}O$, and SP, for N_2O concentrations ranging from 0.5 to 90 ppm as reported by the OA-ICOS analyser. The dotted lines indicate the range over which N_2O concentration corrections were performed (11 to 13 ppm N_2O).

https://doi.org/10.5194/egusphere-2026-857
Preprint. Discussion started: 27 February 2026

2.2.4 Gas matrix effects of oxygen

In nitrifying zones of WWTPs, pressurized air is injected to oxidize NH_4^+ to NO_2^- and NO_3^-. Consequently, O_2 concentrations in the off-gas are at sub-ambient levels and the volumetric content of persistent gas components such as N_2 and Ar is enhanced since any produced CO_2 is removed prior to analysis. We therefore tested the dependence of reported N_2O concentration and δ-values on O_2 concentration in the gas matrix. For this a Cal1 was dynamically mixed with N_2O free dilution air, and high purity N_2 (99.999 %, Linde Gas AG, Switzerland) to incrementally vary the O_2 concentration in the analyte gas from 4 to 20.95 %, while N_2O concentrations were held constant at 12 ppm. Gas mixtures were prepared at a flow rate of 300 mL min^{-1}, and each sample was analysed for ten minutes. To account for any analyser drift, in between every O_2 concentration step, the Cal1 gas was measured at ambient O_2 concentrations (20.95 % O_2). The O_2 concentration dependence of apparent δ-values was constant over the entire range of O_2 concentrations (4 to 20.95 %; Fig. 3), with values of 1.45, 1.57, 1.51, 1.76, and -0.12 ‰ [% O_2]$^{-1}$ for $\delta^{15}N^{\alpha}$, $\delta^{15}N^{\beta}$, $\delta^{15}N^{bulk}$, $\delta^{18}O$, and SP, respectively. Oxygen concentrations in the reactors' off-gas ranged from 19.8 to 20.95 % over the entire 1-year experimental period (O_2 concentrations were measured by PG-350E, Horiba, Japan). The average O_2 concentration in the actual analyte gas is somewhat higher at 20.6 (±0.2) % as the off-gas is diluted with high-purity SA (see above) to set the N_2O concentration to 12 ppm. To account for a systematic reduction in O_2 concentrations by 0.35 %, $\delta^{15}N^{\alpha}$, $\delta^{15}N^{\beta}$, $\delta^{15}N^{bulk}$, $\delta^{18}O$, and SP values were corrected for 0.56, 0.53, 0.55, 0.83, and 0.04 ‰, respectively by using the linear models in Fig. 3. The variability in O_2 concentrations was considered in the uncertainty budget.

https://doi.org/10.5194/egusphere-2026-857
Preprint. Discussion started: 27 February 2026

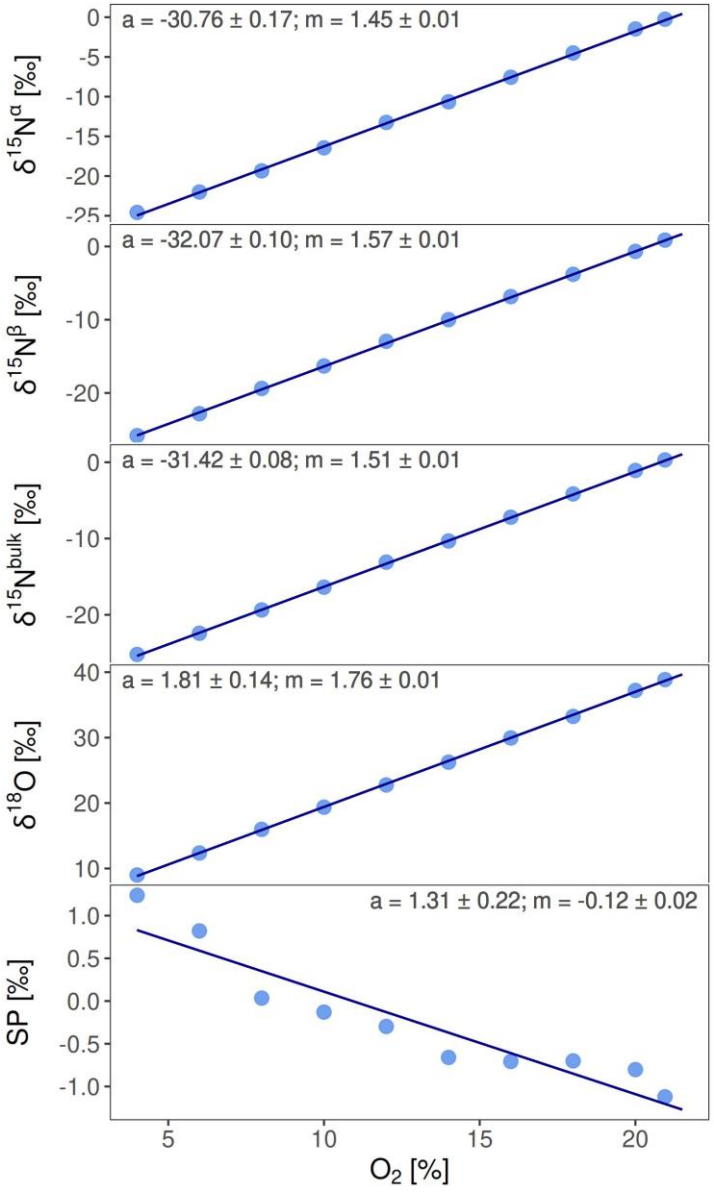

195 Figure 3: Oxygen concentration dependence of apparent δ-values, $\delta^{15}N^{\alpha}$, $\delta^{15}N^{\beta}$, $\delta^{15}N^{bulk}$, $\delta^{18}O$, and SP in N_2O, for O_2 concentrations in the gas matrix ranging from 4 to 20.95 %. Intercept (a) and slope (m) with corresponding standard errors.

2.3 Data processing

Data processing was performed using a MATLAB script adapted from Havsteen et al. (2025) (MATLAB version R2022b Update 3). This script was used to import spectrometer data as well as combine measurement data with label of the analyte
200 gas identity (reactor 1 / 2, Cal1, Cal2). Analyte labels provide start/end times for each measurement interval. The last 5

https://doi.org/10.5194/egusphere-2026-857
Preprint. Discussion started: 27 February 2026

minutes of each interval, when concentrations and δ-values reached, a plateau were used to calculate average N_2O concentrations ($[N_2O]_{sa,av}$), δ-values, and their standard deviations. For further data quality assurance, any averaged δ-values with a standard deviation > 5 ‰ was disregarded from further data processing (4.1 % of total data). To correct for N_2O mole fraction dependence, and for data visualization RStudio (2025.05.1, R version 4.5.1, R Core Team, 2025) and the packages ggplot2 and datatable were used (Barrett et al., 2025; Wickham, 2016).

The raw δ-values provided by the analyser (δ_{Sample}^{Raw}) were corrected for drift ($\Delta\delta_{Drift}$), N_2O mole fraction dependence ($\Delta\delta_{N2O}$) and the dependence of apparent delta values on the O_2 concentration ($\Delta\delta_{O2}$):

$$\delta_{Sample}^{Corr} = \delta_{Sample}^{Raw} - \Delta\delta_{Drift} - \Delta\delta_{N_2O} - \Delta\delta_{O2} \quad (2)$$

Since CO_2 was systematically removed prior to analysis, no correction for CO_2 spectral interferences relevant for the applied OA-ICOS analyser (Harris et al., 2020) was implemented. Analyser drift was monitored and corrected by regular analysis of reference gas Cal1 (Havsteen et al., 2025). For each sample interval, the drift-related offset was determined by subtracting the overall mean of all Cal1 intervals ($\delta_{Cal1}^{Mean,Raw}$) from the linear interpolation of δ-values of the two nearest bracketing Cal1 intervals ($\delta_{Cal1}^{\int(+)}$ and $\delta_{Cal1}^{\int(-)}$):

$$\Delta\delta_{Drift} = \frac{\delta_{Cal_1}^{\mathrm{Int}(-),Raw}\cdot\left(t_{sample}-t_{Cal_1}^{\mathrm{Int}(-)}\right)+\delta_{Cal_1}^{\mathrm{Int}(+),Raw}\cdot\left(t_{Cal_1}^{\mathrm{Int}(+)}-t_{sample}\right)}{t_{Cal_1}^{\mathrm{Int}(+)}-t_{Cal_1}^{\mathrm{Int}(-)}} - \delta_{Cal_1}^{Mean,Raw} \quad (3)$$

The N_2O mole fraction dependence of δ-values was corrected using quadratic correction functions (Fig. 2):

$$\Delta\delta_{N_2O} = b\left([N_2O]_{sa,av} - [N_2O]_{Cal1}\right) + c([N_2O]_{sa}^2 - [N_2O]_{Cal1}^2) \quad (4)$$

where b and c represent fitting parameters of the quadratic correction function and N_2O, $[N_2O]_{Cal1}$ the observed N_2O concentration of the sample and Cal1 gas.

With respect to the O_2 concentration correction of δ-values an offset correction to average O_2 concentrations in the analyte gas (20.6 % O_2) was applied, instead of a correcting for each individual O_2 concentration value (Fig. 3):

$$\Delta\delta_{O_2} = m_{O_2}\left([O_2]_{sa,avg} - [O_2]_{Cal1}\right) \quad (5)$$

where m_{O_2} represents the slope of the respective linear correction function and $[O_2]_{sa,avg}$, $[O_2]_{Cal1}$ are the average O_2 concentration of the analyte gas and Cal1.

Corrected delta values (δ_{Sample}^{Corr}) were calibrated ($\delta_{Sample}^{Corr,Calib}$) as follows:

$$\delta_{Sample}^{Corr,Calib} = y \cdot \left(\delta_{Sample}^{Corr} - \delta_{Cal_1}^{Mean,Corr}\right) + \delta_{Cal_1}^{True} \quad (6)$$

$$y = \frac{\left(\delta_{Cal_1}^{True}-\delta_{Cal_2}^{True}\right)}{\delta_{Cal_1}^{Mean,Corr}-\delta_{Cal_2}^{Mean,Corr}} \quad (7)$$

where $\delta_{Cal_1}^{True}$ and $\delta_{Cal_2}^{True}$ represent the "true" δ-values of the applied reference gases.

https://doi.org/10.5194/egusphere-2026-857
Preprint. Discussion started: 27 February 2026

2.3.1 Fraction of reduced nitrous oxide

Based on the isotopic signatures, the fraction of residual N_2O ($resN_2O_i$) for a SP or $\delta^{18}O$ value (δ_i) was estimated quantitatively by reformulating Eq. 1 to:

$$resN_2O_i = e^{(\delta_{Ri}-\delta_{0i})/\varepsilon_i} \quad (9)$$

where δ_{Ri} is the isotopic signature of the residual N_2O fraction representing individual measurements of either SP or $\delta^{18}O$, δ_{0i} is the isotopic signature of the initial N_2O_i (SP or $\delta^{18}O$) not yet affected by reduction, and ε_i is the enrichment factor (i.e. ε_{SP} = -5.9 ‰ and $\varepsilon_{\delta 18O}$ = -15.4 ‰; Yu et al., 2020).

Values of $\delta 0_i$ were estimated for SP and $\delta^{18}O$ by restricting candidate observations to the lower-left region of the bivariate distribution by ranking observations according to the sum of their $\delta^{18}O$ and SP ranks and retaining the five lowest-ranked points. Further, the perpendicular distance of each of the lowest-ranked observations in the SP and $\delta^{18}O$ space to the reduction line was calculated and the observations with the smallest distance selected. The corresponding $\delta^{18}O$ value was defined as $\delta 0_{18O}$, and the associated $\delta 0_{SP}$ value was obtained by evaluating the regression line at $\delta 0_{18O}$ (Fig. A1). The fraction of reduced N_2O ($redN_2O$) was calculated as the average of the estimates based on SP ($resN_2O_{SP}$) and $\delta^{18}O$ ($resN_2O_{\delta 18O}$): $redN_2O = 1 - (resN_2O_{SP} + resN_2O_{\delta 18O}) / 2$. Here, we used SP and $\delta^{18}O$ as input variables to calculate $redN_2O$, as SP is independent of the isotopic signature of the source and $\delta^{18}O$ was equilibrated to the $\delta^{18}O$ signature of the local tap water. Signatures of $\delta^{15}N^{bulk}$ however, are dependent on the isotopic signature of the substrate and may vary over the course of the aeration time and was therefore not used to calculate redN2O.

2.3.2 Uncertainty assessment

The total uncertainty associated with the corrected δ-values (σ_i) was assessed by combining uncertainty contributions from (i) the N_2O mole fraction correction (σ_{N2Oi}), (ii) the correction for the gas matrix effect of O_2 (σ_{O2i}), and (iii) the repeatability of the instrument ($\sigma_{rep\ i}$). To do so, the law of error propagation was applied on the respective correction functions.

The uncertainty of the N_2O mole fraction correction was estimated from the uncertainty in the quadratic correction function. For this the 95th confidence interval of the fit was chosen at a mean N_2O concentration of 12 ppm. In contrast, the uncertainty related to the correction of the O_2 gas matrix effect was assumed to be dominated by the variability of O_2 concentrations in the actual analyte gas (20.6 ± 0.2 %). Individual uncertainty contributions are shown in Tab. 2. To obtain the total uncertainty of the corrected isotope values the individual contributions were combined in quadrature:

$$\sigma_i = \sqrt{(\sigma_{N2Oi}^2 + \sigma_{O2i}^2 + \sigma_{repi}^2)} \quad (8)$$

The combined uncertainty (σ_i) represents the 1-sigma uncertainty of the final corrected δ-value. Combined uncertainties were 0.85, 1.08, 0.81, 0.48, and 1.09 ‰ for $\delta^{15}N^{\alpha}$, $\delta^{15}N^{\beta}$, $\delta^{15}N^{bulk}$, $\delta^{18}O$, and SP respectively (see Tab. 2).

https://doi.org/10.5194/egusphere-2026-857
Preprint. Discussion started: 27 February 2026

The uncertainty estimate for the residual N_2O fraction (after N_2O reduction) was provided, propagating the uncertainty of SP and $\delta^{18}O$ (N_2O) following first-order Taylor expansion:

$$\sigma_{redN_2O_i} = \frac{\sigma_i}{|\varepsilon| \cdot \sqrt{n}} \quad (9)$$

Table 2: Uncertainty contributions to the total uncertainty of corrected δ-values originating from N_2O mole fraction correction, gas matrix effects and repeatability.

	$\delta^{15}N^{\alpha}$ [‰]	$\delta^{15}N^{\beta}$ [‰]	$\delta^{15}N^{bulk}$ [‰]	$\delta^{18}O$ [‰]	SP [‰]	Comment
N_2O mole fraction correction	0.74	0.53	0.57	0.24	0.61	Dominated by uncertainty in correction function
Gas matrix effects of O_2	0.29	0.31	0.30	0.35	0.02	Uncertainty in O_2 concentration
Repeatability	0.31	0. 89	0.49	0.21	0.90	Derived from repeated measurements of the target gas
Total uncertainty	**0.85**	**1.08**	**0.81**	**0.48**	**1.09**	

2.4 Implementing real-time nitrous oxide isotope analysis at a wastewater treatment plant

2.4.1 Dynamic dilution system

As the apparent δ-values reported by the OA-ICOS analyser are subject to a strong, time-variant N_2O concentration dependence, as discussed in sect. 2.2.3, we decided to implement a dynamic dilution system (Fig. 4) using N_2O-free SA as dilutant to limit uncertainty contributions from N_2O non-linearity corrections. The target concentration of the dilution system was set to 12 ppm N_2O and data with N_2O concentrations outside the range of 11 to 13 ppm were discarded. Data passing this criterion were corrected for non-linearity using average correction functions (Fig. 2).

The custom-built dilution system consisted of five mass flow controllers (MFC; Vögtlin Instruments GmbH, Switzerland), automated by a customized LabView programme (National Instruments, USA). Four MFCs were used to control flows of the analyte gas, Cal1, Cal2 and N_2O-free SA to dilute the analyte gas to the target N_2O concentration. One additional MFC set to 400 mL min^{-1} was used to maintain a constant flow of analyte gas during Cal1 and Cal2 measurements to reduce lag times during subsequent analyte gas measurements (Fig. 4). The dilution ratio and MFC flow rates were calculated based on a 20 second running average of the actual N_2O concentration in the off-gas of the reactor provided by a NDIR analyser (X-STREAM X2XF, Rosemount Emerson, USA). The analyte gas was provided to the regulating MFC at 2.5 bar overpressure using a membrane pump (N86, KNF Holding AG, Switzerland). The intake of the pump was restricted with a needle valve,

https://doi.org/10.5194/egusphere-2026-857
Preprint. Discussion started: 27 February 2026

while the overpressure downstream of the membrane pump was monitored and manually adjusted with a pressure relief valve. To maintain stable operation of the MFC a critical orifice (bore diameter 150 µm) was installed in between membrane pump and MFC dampening pressure oscillations. The analyte gas was dehumidified by permeation drying (MD-070, Perma Pure, USA), CO_2 removed by absorption (Ascarite, mesh size 20-30; Sigma Aldrich, USA) and particles eliminated using an in-line sintered metal filter (pore size 2 µm; Swagelok, USA). Part of the analyte gas was supplied to the OA-ICOS spectrometer (about 200 mL min^{-1}), and the remainder (about 200 ml min^{-1}) exhausted to ambient air passing a NDIR CO_2 sensor (Sensair HPP, Sweden), to detect breakthrough of the CO_2 trap.

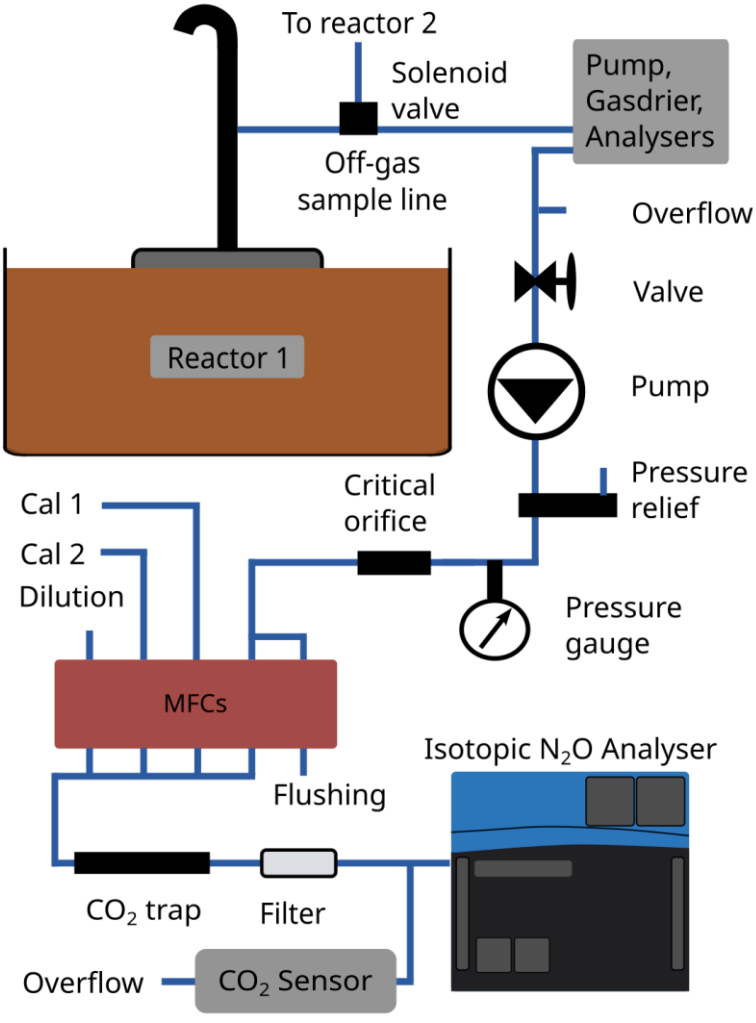

Figure 4: Schemata of the experimental set-up applied for alternate sampling the off-gas of two wastewater treatment reactors and real time analysis of N_2O concentration and isotopic composition using an OA-ICOS spectrometer. The analyte gas treatment includes sequential dehumidification, dilution using MFCs (mass flow controllers), CO_2 removal and particle

https://doi.org/10.5194/egusphere-2026-857
Preprint. Discussion started: 27 February 2026

filtering. The CO_2 sensor is implemented to monitor quantitative CO_2 removal and thus the absence of CO_2 spectral interferences.

2.5 Experiments at a pilot-scale wastewater treatment plant

Real-time analysis of N_2O concentration and isotope δ-values was performed at two pilot-scale wastewater treatment reactors (volume per reactor: 8 m^3) operated by Eawag in Dübendorf, Switzerland. The reactors received the same local municipal wastewater and were run as sequencing batch reactors in parallel. Each cycle consisted of an anoxic feeding phase, an aeration phase with duration controlled by NH_4^+ concentration, a settling phase, and a discharge period with 25 to 55 % volume exchange. After each cycle, the remaining sludge of both reactors was mixed to ensure a comparable microbiome between the two reactors (Strubbe et al., 2026).

To distinguish between N_2O production pathways, we analysed the N_2O isotopic composition in the reactors' off-gas during the aeration phases. Experiments were conducted over a period of 12 months with 998 hours of measurement time. While this study focuses on performance and usability of the described analytical setup and corresponding methodological aspects, follow up manuscripts will address more specific wastewater treatment related research questions in detail (e.g. Strubbe et al., 2026). Following representative datasets obtained under three different experimental conditions are showcased here to demonstrating usability and applicability of our analytical setup:

i) To determine the predominant N_2O biological production pathway, we analysed the N_2O isotopic composition over several months (June to December 2024) under standard operation, i.e. at a dissolved O_2 (DO) concentration setpoint of 2 mg L^{-1} (±0.5 mg L^{-1}) and without N-substrate additions.

ii) To assess the usability of our on-line isotopic measurement setup in capturing relevant process dynamics, we designed experiments in which the DO concentration was varied between reactors while all other parameters remained constant. This allowed us to investigate effects of different DO concentrations on microbial pathways and N_2O reduction. In short, we ran one reactor at a DO concentration of 2 mg L^{-1}, while the second was run at a DO concentration of 0.5 mg L^{-1}. At the start of the aeration phase, each reactor received 118 g $NaNO_2$ (targeting 3 mg N L^{-1} in the reactor) to stimulate N_2O production. Beforehand, the $\delta^{18}O\text{-}NO_2^-$ of the $NaNO_2$ solutions was set by equilibrating (74 hours at 40°C, 74 hours at reactor temperature) with the local tap water ($\delta^{18}O_{H2O}$ = -11.2 ‰).

iii) As a third application of our on-line isotopic measurement setup, we investigated its usability for low-level ^{15}N-labelling, a novel methodology that uses the addition of small amounts of labelled substrate to increase δ-values to a level above natural abundance but low enough to still allows the use of natural abundant fractionation factors as well as standard isotopic measurement methods (Deb et al., 2025). This method is very valuable to investigate N-transformation processes and nD and hD activity during different operational conditions. We therefore performed a low-level ^{15}N-labelling experiment in one of our reactors. In short, the following procedure was applied: At the beginning of the aeration phase the reactor was depleted

https://doi.org/10.5194/egusphere-2026-857
Preprint. Discussion started: 27 February 2026

of NH_4^+, by setting the DO concentration to 6 mg L^{-1} until the NH_4^+ concentration was below detection limit of the NH_4^+ sensor (COS61, ISEmax CAS40, Endress+Hauser, Switzerland). Then, the DO concentration setpoint was reduced to 4 mg L^{-1}, and the NO_3^- concentration increased to 10 mg N L^{-1} by adding $NaNO_3$. Additionally NH_4^+ concentrations were increased to 10 mg N L^{-1} by adding ^{15}N-labelled NH_4^+, to set $\delta^{15}N_{NH4+}$ in the reactor to approx. 100 ‰. The duration of the aeration phase was manually set to 3 hours, during which the N_2O isotopic composition was monitored. During the subsequent cycle, i.e. after an exchange of 60 % of the clean effluent with fresh municipal wastewater, the DO setpoint was reduced to 2 mg L^{-1} and no substrates were added. Again, the isotopic composition was analysed during the aeration phase.

https://doi.org/10.5194/egusphere-2026-857
Preprint. Discussion started: 27 February 2026

3. Results and Discussion

3.1 Performance of the measurement setup

The dynamic dilution system reliably diluted the reactor off-gas to a target concentration of approximately 12 ppm (Fig. 5, note that the figure shows raw data, i.e. prior to calibration and corrections). It performed particularly well if N_2O concentrations in the reactor off-gas were consistent throughout the measurement interval. Initially, under rapid concentration changes, particularly at high N_2O concentrations (above approx. 100 ppm), however, the off-gas transfer from the N_2O concentration analyser to the dilution system occasionally lagged. This led to enhanced variability in the analyte N_2O concentration and partly to invalid isotope data due to N_2O concentrations outside the 11 to 13 ppm N_2O range. The situation was improved by increasing the gas flow rate and implementing an additional mass flow controller to flush the sample stream during Cal1 measurements between each sample analysis (Fig. 4). Another challenge throughout the experimental period was maintaining consistent CO_2 removal rates, as the absorbent traps regularly showed CO_2 breakthrough before the actual trap capacity was reached. We assume the occurrence of preferential flow paths to be responsible for this. As all data acquired during breakthrough periods were discarded, data quality was not compromised. A possible strategy to avoid future data loss could be the more frequent automated change of traps as integrated by Ibraim et al., (2019) or the development of an alternative dual-trap system with regenerative adsorbent.

Despite some challenges, the integrated on-line isotopic analysis offers significant advantages over discrete sampling methods. Continuous monitoring provides high temporal resolution, capturing short-term fluctuations and dynamic processes, providing data that enables more accurate characterization of N_2O emission patterns and diurnal cycles and reduces uncertainty associated with interpolation between sparse data points. Additionally, on-line systems avoid artifacts from incorrect sample storage, which may lead to increased uncertainties due to fractionation effects or even sample loss. With minor adaptations the here introduced isotopic measurement setup will be capable of performing long-term measurements at full-scale WWTPs to provide on-line data that enables direct control in on-site mitigation efforts.

https://doi.org/10.5194/egusphere-2026-857
Preprint. Discussion started: 27 February 2026

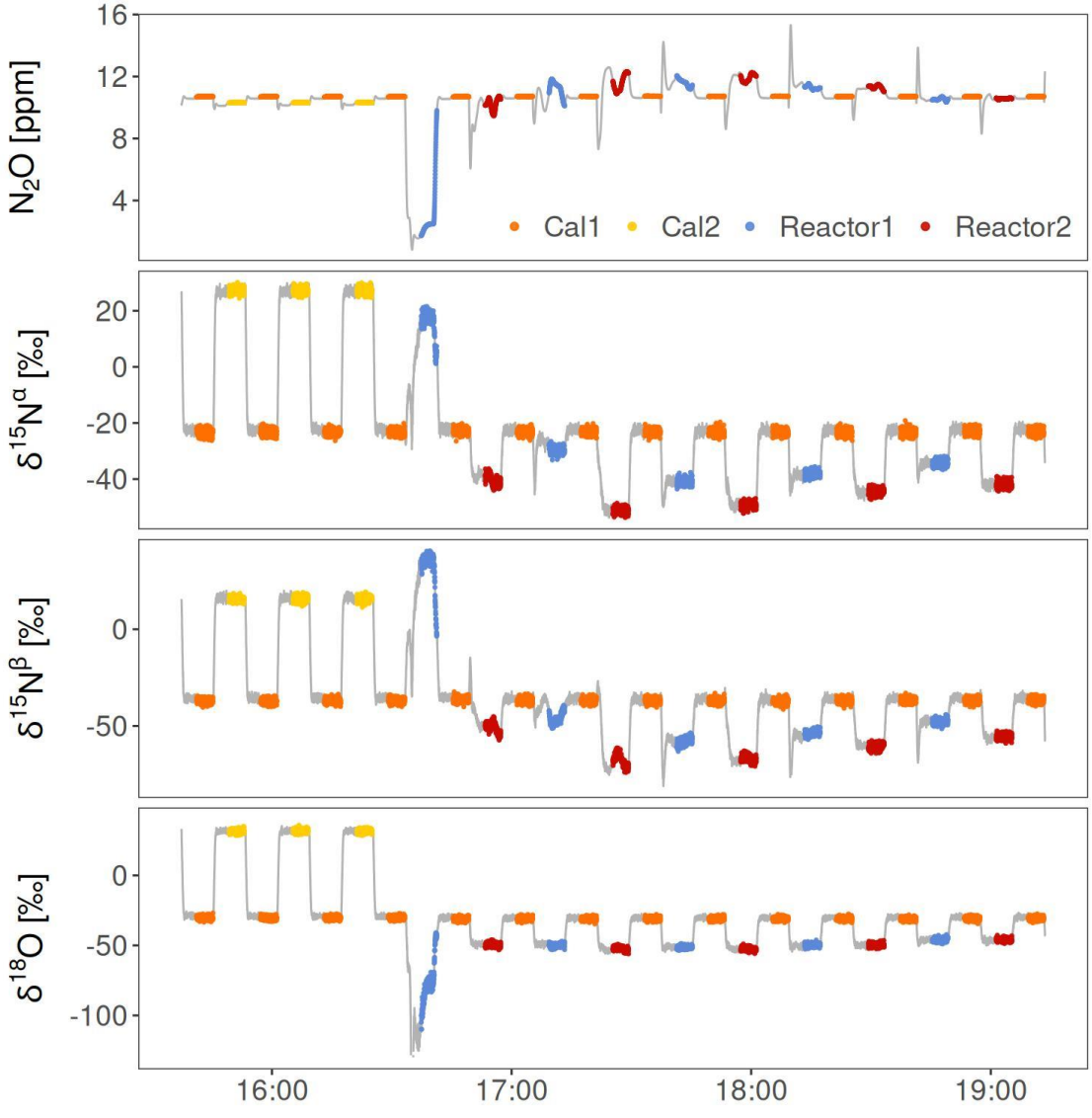

Figure 5: N_2O concentration data and $\delta^{15}N^{\alpha}$, $\delta^{15}N^{\beta}$, $\delta^{18}O$ values as provided by the laser spectrometer, i.e. prior to corrections and calibration. Data from June 12th 2025 under standard operation conditions. A measurement interval of 8 minutes was chosen and only the last five minutes of each interval were used for further analysis to assure complete exchange of the analyte gas in the gas pretreatment and analyser. Cal1 measurements are shown in orange, Cal2 measurements in yellow and sample measurements in blue (reactor 1) and red (reactor 2).

3.2 Representative data sets demonstrating system applicability

3.2.1 Constraining nitrous oxide production pathways under standard operation

Figure 6 displays the N_2O isotopic composition during standard operation of the two wastewater treatment reactors presented as a dual isotopic plot of SP versus $\delta^{18}O$ (N_2O) values, after data processing (section 2.3). Isotopic signatures of relevant

https://doi.org/10.5194/egusphere-2026-857
Preprint. Discussion started: 27 February 2026

production processes (Hy, nD, and hD) derived from laboratory studies are indicated as rectangular shaded areas for comparison (Yu et al., 2020). The $\delta^{18}O$ (N_2O) values were corrected for the $\delta^{18}O$ signature of the local tap water, and plotted as $\Delta\delta^{18}O$ (N_2O, H_2O) = $\delta^{18}O$ (N_2O) - $\delta^{18}O$ (H_2O). Concurrent changes in SP and $\Delta\delta^{18}O$ (N_2O, H_2O) along a straight line with a slope of 0.37 indicate successive reduction of N_2O to N_2 (Yu et al., 2020). From this plot we can infer nitrifier or heterotrophic denitrification as the dominant N_2O production process, as measurements fall within the range of isotopic signatures expected for denitrification processes with a minimal effect of N_2O reduction (Yu et al., 2020) and are in accordance with other studies on wastewater treatment (Gruber et al., 2022; Wunderlin et al., 2013). Furthermore, the absence of elevated SP values (> 30‰) suggests that Hy was not a source term during our measurements (Frame and Casciotti, 2010; Sutka et al., 2006; Wunderlin et al., 2013; Yu et al., 2020). To robustly differentiate between the contributions of nD and hD to N_2O formation requires further dedicated experiments that aim at stimulating both processes independent from each other. A series of such experiments applying the analytical toolkit developed in this study is described in Strubbe et al. (2026). The source signatures indicated as shaded areas in Fig. 6 are based on a limited number of pure culture studies and laboratory incubations (Yu et al., 2020) and therefore require refinement to fully capture the dynamics of complex mixed microbial communities as are found in wastewater treatment reactors. Furthermore, the borders and overlaps of the different source signature areas will likely be subject to change with increased understanding of the complexities of managed and natural N_2O source systems.

https://doi.org/10.5194/egusphere-2026-857
Preprint. Discussion started: 27 February 2026

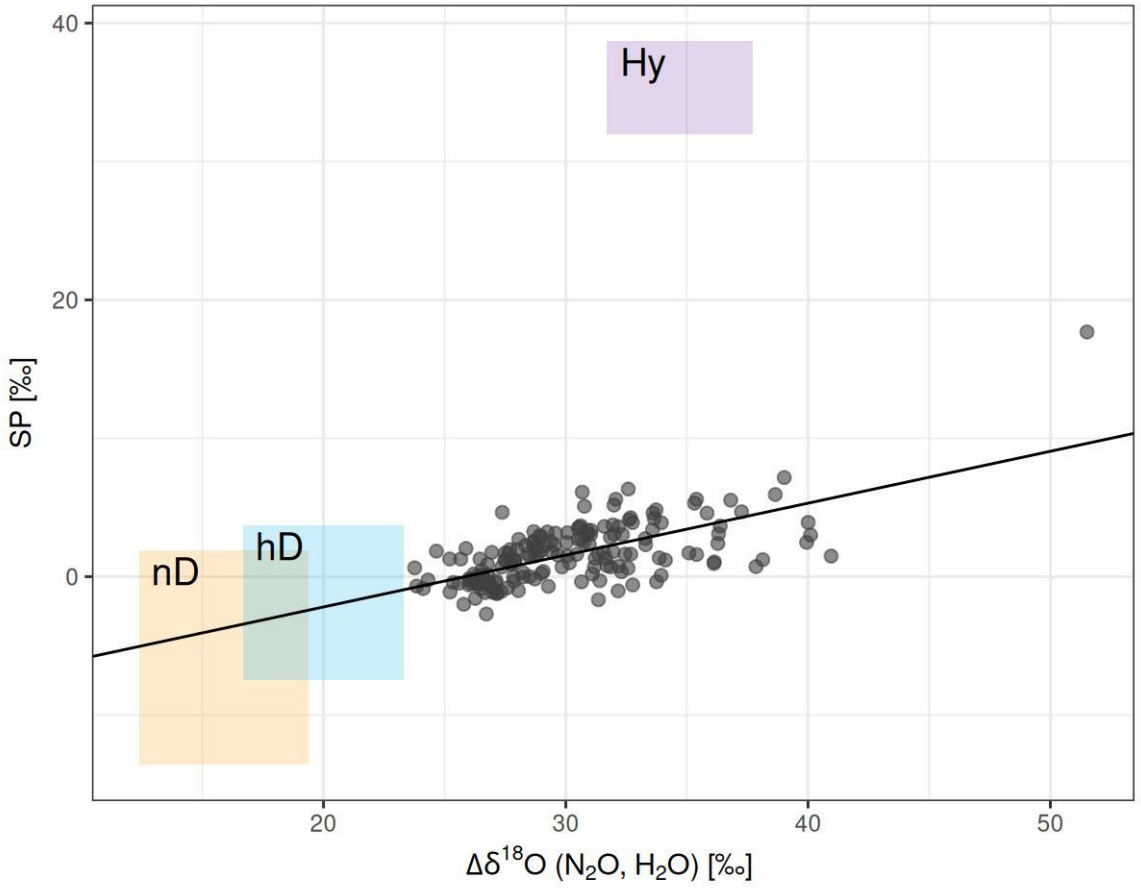

Figure 6: Dual-isotope plot of SP and $\Delta\delta^{18}O$ (N_2O, H_2O) measured during standard operations of wastewater treatment (data from June to December 2024, n = 170). Total uncertainties are 1.09 ‰ for SP and 0.48 ‰ for $\delta^{18}O$ (N_2O). Coloured boxes indicate expected source signatures of N_2O production pathways without fractionation effects from partial N_2O to N_2 reduction (Yu et al., 2020). The linear regression (black line; slope of 0.37) represents the so-called "reduction line", i.e. the progressive increase in SP and $\delta^{18}O$ with progressive N_2O reduction. (Hy: hydroxylamine oxidation, nD: nitrifier denitrification, hD: heterotrophic denitrification).

3.2.2 Assessing the degree of nitrous oxide reduction as a function of dissolved oxygen concentration

During heterotrophic N_2O reduction to N_2, the N_2O molecule is preferentially split between the N-O bond of lighter isotopes, leading to an enhancement in $\delta^{15}N^{bulk}$, SP, and $\delta^{18}O$ in the remaining N_2O pool (Lewicka-Szczebak et al., 2017; Ostrom et al., 2007). The enrichment of SP, and $\delta^{18}O$ due to N_2O reduction leads to a characteristic slope reported to span from 0.23 to

https://doi.org/10.5194/egusphere-2026-857
Preprint. Discussion started: 27 February 2026

0.98 (Yu et al., 2020) that defines the reduction line (Fig. 7 and Fig. A1). The slope of our reduction line (0.80; Fig. 7A) falls within the range reported in the literature, supporting the validity of the here reported N_2O reduction fractions.

Dissolved O_2 concentration was identified as an important driver of N_2O to N_2 reduction by hD (Fig. 7B). The low DO concentration setpoint of 0.5 mg L^{-1} led to an increase in the fraction of reduced N_2O by 33 % (±2 %) compared to the DO setpoint of 2 mg L^{-1}. The wastewater treatment reactor set to low DO showed an increasing trend in redN2O from 31 to 42 % followed by a decline to 33 % over the course of the experiment. In contrast, the reactor set to high DO displayed a steady decrease in the redN_2O from 8 to 0 %. The substantial difference between the two treatments can be explained by the O_2-sensitive nature of the enzyme responsible for N_2O reduction (Pomowski et al., 2011). These findings align with previous studies demonstrating that low O_2 concentrations enhance N_2O reduction efficiency and vice-versa (Morley et al., 2008; Suenaga et al., 2018; Tang et al., 2022; Zhou et al., 2021). Different O_2 concentration thresholds were found to trigger N_2O reduction, Tang et al. (2022) found the N_2O reduction rate to increase exponentially with decreasing O_2 concentration below a threshold of 1.6 mg O_2 L^{-1} in estuarine waters. Whereas, Rees et al. (2021) reported that in marine water samples, N_2O consumption was observed at O_2 concentrations as high as 8 mg O_2 L^{-1} and Körner and Zumft (1989) reported a threshold of 5 mg O_2 L^{-1} below which N_2O reductase expression was enhanced. This high variability of reported thresholds may be related to species or community dependencies in the response of N_2O reduction to O_2 concentrations (Cavigelli and Robertson, 2001; Suenaga et al., 2018; Zhou et al., 2021). The type and availability of organic carbon represents another control on N_2O reduction, which likely controlled the decrease in N_2O reduction over time, particularly at the high DO setpoint (Azam et al., 2002; Liu et al., 2022; Morley and Baggs, 2010).

https://doi.org/10.5194/egusphere-2026-857
Preprint. Discussion started: 27 February 2026

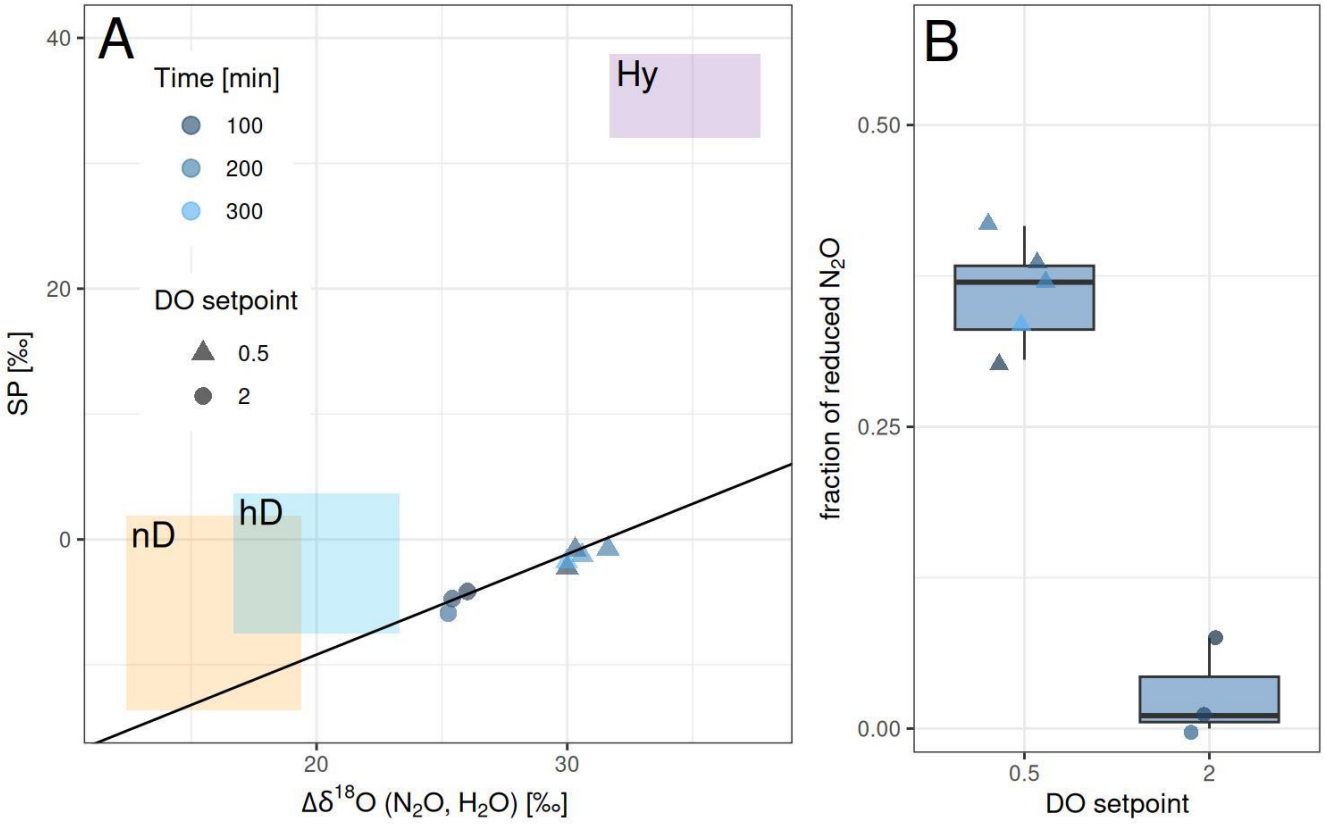

Figure 7: A: Dual-isotope plot of SP and $\Delta\delta^{18}O$ (N_2O, H_2O) measured during experiments with distinctly different dissolved O_2 (DO) content in both reactors. Coloured boxes indicate expected source signatures of N_2O production pathways without N_2O to N_2 reduction (Yu et al., 2020), the linear regression (black line; slope of 0.80) represents the "reduction line". (Hy: hydroxylamine oxidation, nD: nitrifier denitrification, hD: heterotrophic denitrification). B: comparison of the fraction of reduced N_2O (redN_2O) for the two DO setpoints. Uncertainties for redN_2O are estimated to be 2 %. The colour gradient of the symbols in A and B indicates the time passed since aeration started. The different number of data points for the low DO scenario (n=5) and the high DO scenario (n=3) is due to a longer N_2O production phase at low DO. Data from February 21st 2025.

3.2.3 ^{15}N-labelling experiment

Low-level ^{15}N-labelling is a novel methodology that uses the addition of labelled substrate to slightly increase $\delta^{15}N$ values to a level above natural abundance (100-200 ‰) to achieve clear traceability through biogeochemical reactions, but within a range that still allows the use of natural abundant fractionation factors as well as standard isotopic measurement methods (Deb et al., 2025). Here, the addition of ^{15}N-NH_4 ($\delta^{15}N\text{-}NH_4^+$ = 100 ‰ in the total NH_4^+ pool) at the onset of the aeration phase 1 results in N_2O emissions with distinctly higher $\delta^{15}N^{bulk}$ values compared to the bulk of our measurements outside of the low-level labelling experiments (Fig. 8a). An initial increase in $\delta^{15}N^{bulk}$ to 6.5 ‰ as compared to around -40 ‰ under standard operation is consistent with progressive conversion of ^{15}N-labelled NH_4^+ into NO_2^- and NO_3^-, which act as

https://doi.org/10.5194/egusphere-2026-857
Preprint. Discussion started: 27 February 2026

substrates for N_2O formation (Fig. 8b). After the NH_4^+ is depleted, $\delta^{15}N^{bulk}$ of N_2O stagnates. In the second cycle, after a volume exchange of ca. 38 % and an anoxic feeding phase, denitrification likely converted a large portion of the labelled inorganic ^{15}N nitrogen substrate to N_2O and N_2 of which most was removed from the system but the $\delta^{15}N^{bulk}$ values of -27 ‰ are still slightly elevated compared to standard operation. These results demonstrate the suitability of the on-line isotopic measurement setup for low-level ^{15}N-labelling studies as well as the benefit of labelled substrate addition to isolate contributions from specific microbial conversions to the N_2O that is produced. A more complete quantitative analysis of these results requires considering the $\delta^{15}N$ of aqueous nitrogen species and will be published independently.

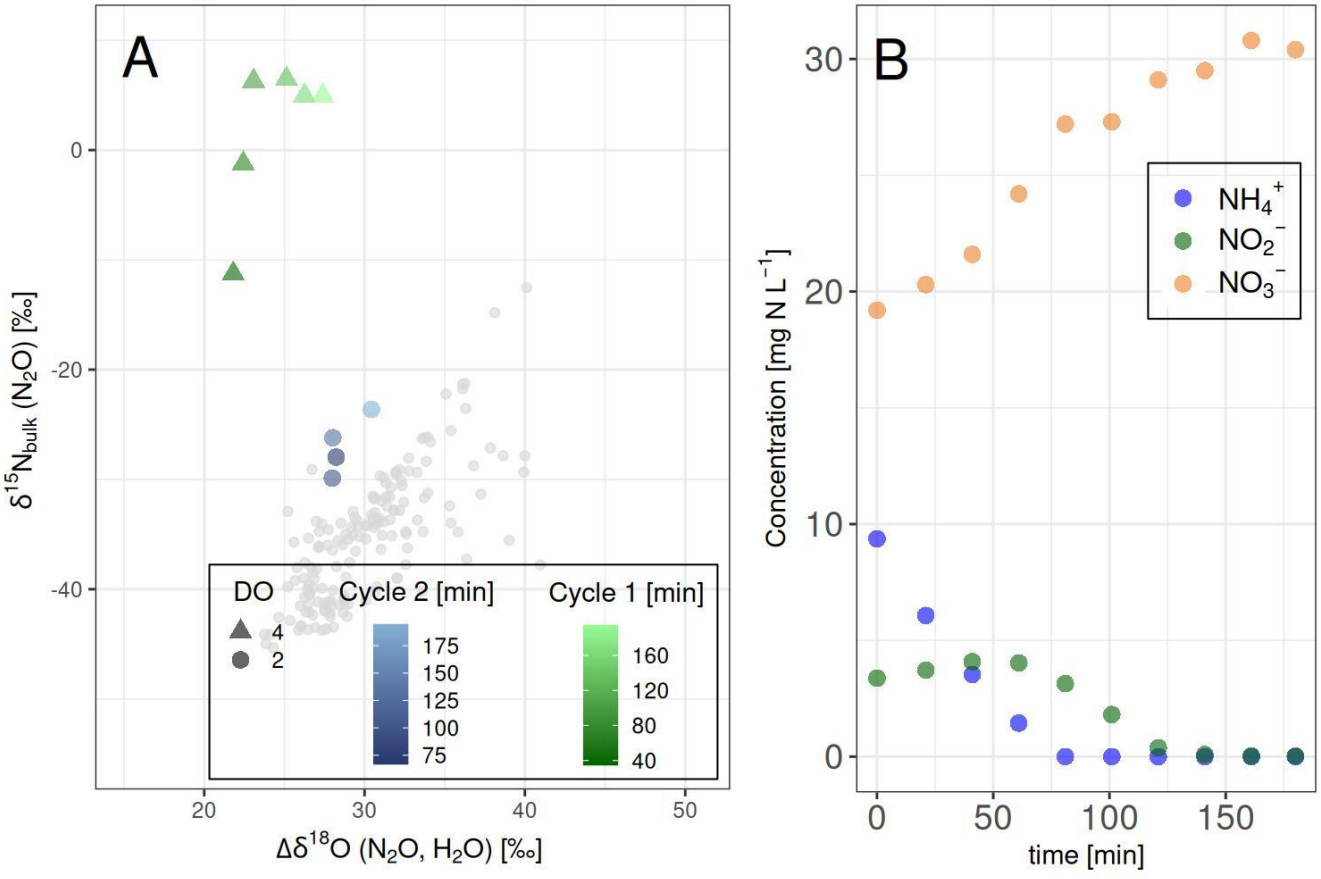

Figure 8: A: Dual-isotope plot of $\delta^{15}N^{bulk}$ and $\Delta\delta^{18}O$ (N_2O, H_2O) measured in a ^{15}N labelling experiment for two consecutive aeration cycles, The first cycle after ^{15}N-NH_4 addition ($\delta^{15}N$-NH_4^+ = 100 ‰) and the second cycle are printed in green and blue, respectively (data from June 10th 2025). Grey dots represent isotopic values during standard operation (data from June to December 2024, n = 170), given for comparison. The colour gradient indicates the time passed since aeration started. B: Temporal trend of ammonium (NH_4^+), nitrate (NO_3^-), and nitrite (NO_2^-) concentration over the course of the first cycle.

https://doi.org/10.5194/egusphere-2026-857
Preprint. Discussion started: 27 February 2026

4. Conclusion

This study demonstrates the feasibility and advantage of real-time N_2O isotopic analysis using off-axis integrated cavity output spectroscopy in a pilot-scale wastewater treatment setting. By implementing a dynamic dilution system and robust correction protocols, we achieved accurate measurements of $\delta^{15}N^{\alpha}$, $\delta^{15}N^{\beta}$, $\delta^{15}N$, $\delta^{18}O$, including ^{15}N site preference, under variable process conditions, most importantly analyte gas composition. Applying a fully-automated setup, with intermittent drift correction, up to three 5-minute averaged gas sample measurements were realized per hour. Continuous monitoring in intermittent campaigns was demonstrated over a one-year study period, pointing out heterotrophic denitrification or nitrifier denitrification as the dominant N_2O source and no signs indicative of hydroxylamine oxidation. Furthermore, the system enabled the assessment of N_2O reduction dynamics and its dependence on process parameters, especially the dissolved O_2 concentration. In a prototype application the analytical setup also proved suitable for ^{15}N labelling experiments, offering new opportunities to study nitrogen transformation dynamics in complex engineered environments at high temporal resolution.

Beyond these initial applications, the platform offers significant potential for in-depth pathway characterisation by isolating contributions from individual microbial processes through targeted stimulation. It can support optimisation strategies by identifying the balance between N_2O production and reduction and quantifying environmental constraints such as pH, carbon availability, micronutrient supply, or microbial composition. Importantly, the approach is not limited to pilot-scale reactors; it can be adapted for on-line monitoring at full-scale wastewater treatment plants, enabling integration into operational control and mitigation frameworks.

These findings underline the potential of laser spectroscopy as a practical tool for process optimisation and emission mitigation in wastewater treatment. Future work should focus on extending this approach to full-scale plants and incorporating isotopic data into advanced control strategies for greenhouse gas reduction.

5. Code and data availability

All raw data and code can be provided upon request to the corresponding authors.

6. Author contributions

HK tested and implemented the on-line isotopic analytic system guided by JM, contributed to the conceptualization of the study and the experimental strategy, performed data acquisition and analysis, and drafted the manuscript. LS operated the pilot reactors, contributed to the experimental strategy, to the interpretation of the results, and by editing the manuscript. PMM supported the conceptualization of the study and the formation of the experimental strategy and contributed to the manuscript by writing and editing. AJ provided the experimental wastewater treatment pilot setup, discussed the experimental strategy and contributed to writing and editing. AF discussed the experimental strategy and contributed to the

https://doi.org/10.5194/egusphere-2026-857
Preprint. Discussion started: 27 February 2026

manuscript by writing and editing. AK developed a solution for automatic calibration and dynamic dilution of the off-gas. KHK made the OA-ICOS available for this study and contributed to the manuscript by writing and editing. JM provided the framework to this study, prepared the calibration gases used in this study and made significant contributions to the conceptualisation as well as to the manuscript by writing and editing.

7. Competing interests

The authors declare no competing interests.

8. Acknowledgements

We thank Marco Kipf, Martin Breitenstein and the team at Eawag's pilot wastewater treatment plant for maintaining reactor operation and for their support during implementation of our on-line analytic system, Roland Werner for $\delta^{18}O$ analysis of our water samples, and Pascal Rubli for providing us with a CO_2 sensor. Christoph Hüglin, Stephan Henne, Liu Ye, Kristie Boering, and Lukas Emmenegger provided valuable input to conceptualization, data interpretation and analysis.

9. Financial support

The project is part of Empa's and Eawag's contribution to the Swiss Center of Excellence on Net-Zero Emissions (SCENE), a joint initiative of all six institutions of the ETH Domain, which is partly funded by the ETH Board.

https://doi.org/10.5194/egusphere-2026-857
Preprint. Discussion started: 27 February 2026

10. Appendix

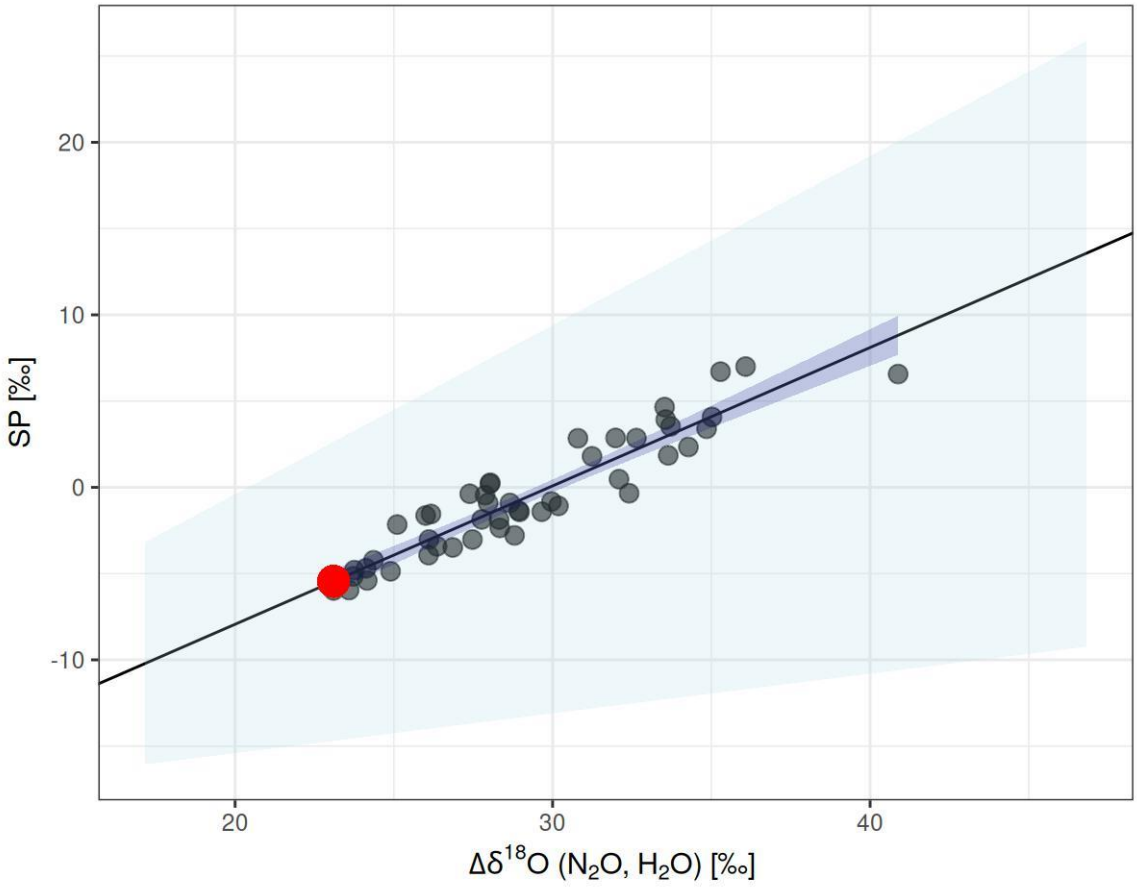

Figure A1: SP plotted against $\Delta\delta^{18}O$ (N_2O, H_2O) with the linear regression line representing the study-specific reduction line. Dark blue area covers the 99 % confidence interval; the light blue area indicates the range of reduction slopes reported in the literature (Yu et al., 2020); the red dot represents δ_0 as estimated by the method described in section 2.3.1. Data from February 5th to February 21st 2025; n = 45.

11. References

Allan, D.W., 1966. Statistics of atomic frequency standards. IEEE 54, 221–230.

Azam, F., Müller, C., Weiske, A., Benckiser, G., Ottow, J., 2002. Nitrification and denitrification as sources of atmospheric nitrous oxide - role of oxidizable carbon and applied nitrogen. Biol. Fertil. Soils 35, 54–61. https://doi.org/10.1007/s00374-001-0441-5

https://doi.org/10.5194/egusphere-2026-857
Preprint. Discussion started: 27 February 2026

Baer, D.S., Paul, J.B., Gupta, M., O'Keefe, A., 2002. Sensitive absorption measurements in the near-infrared region using off-axis integrated-cavity-output spectroscopy. Appl. Phys. B Lasers Opt. 75, 261–265. https://doi.org/10.1007/s00340-002-0971-z

BAFU, 2025. Entwicklung der Treibhausgasemissionen der Schweiz seit 1990.

Barrett, T., Dowle, M., Srinivasan, A., Gorecki, J., Chirico, M., Toby Hocking, Benjamin Schwendinger, Ivan Krylov, 2025. data.table: Extension of `data.frame`.

Camin, F., Besic, D., Brewer, P.J., Allison, C.E., Coplen, T.B., Dunn, P.J.H., Gehre, M., Gröning, M., Meijer, H.A.J., Hélie, J.-F., Iacumin, P., Kraft, R., Krajnc, B., Kümmel, S., Lee, S., Meija, J., Mester, Z., Mohn, J., Moossen, H., Qi, H., Skrzypek, G., Sperlich, P., Viallon, J., Wassenaar, L.I., Wielgosz, R.I., 2025. Stable Isotope Reference Materials and Scale Definitions—Outcomes of the 2024 IAEA Experts Meeting. Rapid Commun. Mass Spectrom. 39, e10018. https://doi.org/10.1002/rcm.10018

Cavigelli, M.A., Robertson, G.P., 2001. Role of denitrifier diversity in rates of nitrous oxide consumption in a terrestrial ecosystem. Soil Biol. Biochem. 33, 297–310. https://doi.org/10.1016/S0038-0717(00)00141-3

Daelman, M.R.J., van Voorthuizen, E.M., van Dongen, U.G.J.M., Volcke, E.I.P., van Loosdrecht, M.C.M., 2015. Seasonal and diurnal variability of N2O emissions from a full-scale municipal wastewater treatment plant. Sci. Total Environ. 536, 1–11. https://doi.org/10.1016/j.scitotenv.2015.06.122

Deb, S., Espenberg, M., Well, R., Bucha, M., Jakubiak, M., Mander, Ü., Jędrysek, M.-O., Lewicka-Szczebak, D., 2025. N transformations in nitrate-rich groundwaters: combined isotope and microbial approach. Biogeosciences 22, 5535–5556. https://doi.org/10.5194/bg-22-5535-2025

Domingo-Félez, C., Jensen, M.M., Bang, A., Smets, B.F., 2024. Variability and Uncertainty Analysis of N_2 O Emissions from WWTP to Improve the Accuracy of Emission Factors and the Design of Monitoring Strategies. ACS EST Water 4, 2542–2552. https://doi.org/10.1021/acsestwater.4c00048

EEA, 2017. Annual European Union greenhouse gas inventory 1990–2015 and inventory report 2017 (No. 6). Copenhagen.

Frame, C.H., Casciotti, K.L., 2010. Biogeochemical controls and isotopic signatures of nitrous oxide production by a marine ammonia-oxidizing bacterium. Biogeosciences 7, 2695–2709. https://doi.org/10.5194/bg-7-2695-2010

Froemelt, A., Zueger, L., von Kaenel, L., Braun, D., Gruber, W., 2025. Pattern recognition of operational states leading to N2O-emissions in full-scale biological wastewater treatment. Water Res. X 29, 100336. https://doi.org/10.1016/j.wroa.2025.100336

Gruber, W., Magyar, P.M., Mitrovic, I., Zeyer, K., Vogel, M., Von Känel, L., Biolley, L., Werner, R.A., Morgenroth, E., Lehmann, M.F., Braun, D., Joss, A., Mohn, J., 2022. Tracing N2O formation in full-scale wastewater treatment with natural abundance isotopes indicates control by organic substrate and process settings. Water Res. X 15, 100130. https://doi.org/10.1016/j.wroa.2022.100130

Gruber, W., Villez, K., Kipf, M., Wunderlin, P., Siegrist, H., Vogt, L., Joss, A., 2020. N2O emission in full-scale wastewater treatment: Proposing a refined monitoring strategy. Sci. Total Environ. 699, 134157. https://doi.org/10.1016/j.scitotenv.2019.134157

Gruber, W., von Känel, L., Vogt, L., Luck, M., Biolley, L., Feller, K., Moosmann, A., Krähenbühl, N., Kipf, M., Loosli, R., Vogel, M., Morgenroth, E., Braun, D., Joss, A., 2021. Estimation of countrywide N2O emissions from wastewater treatment in Switzerland using long-term monitoring data. Water Res. X 13, 100122. https://doi.org/10.1016/j.wroa.2021.100122

Harris, E., Joss, A., Emmenegger, L., Kipf, M., Wolf, B., Mohn, J., Wunderlin, P., 2015. Isotopic evidence for nitrous oxide production pathways in a partial nitritation-anammox reactor. Water Res. 83, 258–270. https://doi.org/10.1016/j.watres.2015.06.040

Harris, S.J., Liisberg, J., Xia, L., Wei, J., Zeyer, K., Yu, L., Barthel, M., Wolf, B., Kelly, B.F.J., Cendón, D.I., Blunier, T., Six, J., Mohn, J., 2020. N_2O isotopocule measurements using laser spectroscopy: analyzer characterization and intercomparison. Atmospheric Meas. Tech. 13, 2797–2831. https://doi.org/10.5194/amt-13-2797-2020

Havsteen, J.C., Fatima, M., Brunamonti, S., Pogány, A., Hausmaninger, T., Wolf, B., Well, R., Mohn, J., 2025. Correction and Calibration Protocol for Isotope Data via CRDS: A Study Case for N_2 O and Other Isotope Systems. https://doi.org/10.5194/egusphere-2025-4954

https://doi.org/10.5194/egusphere-2026-857
Preprint. Discussion started: 27 February 2026

Ibraim, E., Wolf, B., Harris, E., Gasche, R., Wei, J., Yu, L., Kiese, R., Eggleston, S., Butterbach-Bahl, K., Zeeman, M., Tuzson, B., Emmenegger, L., Six, J., Henne, S., Mohn, J., 2019. Attribution of N_2 O sources in a grassland soil with laser spectroscopy based isotopocule analysis. Biogeosciences 16, 3247–3266. https://doi.org/10.5194/bg-16-3247-2019

IPCC, 2021. Climate Change 2021 – The Physical Science Basis: Working Group I Contribution to the Sixth Assessment Report of the Intergovernmental Panel on Climate Change, 1st ed. Cambridge University Press. https://doi.org/10.1017/9781009157896

IPCC, 2019. Chapter 6 Wastewater treatment and discharge, 2019 Refinement to the 2006 IPCC Guidelines for National Greenhouse Gas Inventories.

Kampschreur, M.J., Temmink, H., Kleerebezem, R., Jetten, M.S.M., van Loosdrecht, M.C.M., 2009. Nitrous oxide emission during wastewater treatment. Water Res. 43, 4093–4103. https://doi.org/10.1016/j.watres.2009.03.001

Körner, H., Zumft, W.G., 1989. Expression of Denitrification Enzymes in Response to the Dissolved Oxygen Level and Respiratory Substrate in Continuous Culture of Pseudomonas stutzeri. Appl. Environ. Microbiol. 55, 1670–1676.

Kosonen, H., Heinonen, M., Mikola, A., Haimi, H., Mulas, M., Corona, F., Vahala, R., 2016. Nitrous Oxide Production at a Fully Covered Wastewater Treatment Plant: Results of a Long-Term Online Monitoring Campaign. Environ. Sci. Technol. 50, 5547–5554. https://doi.org/10.1021/acs.est.5b04466

Law, Y., Ye, L., Pan, Y., Yuan, Z., 2012. Nitrous oxide emissions from wastewater treatment processes. Philos. Trans. R. Soc. B Biol. Sci. 367, 1265–1277. https://doi.org/10.1098/rstb.2011.0317

Lewicka-Szczebak, D., Augustin, J., Giesemann, A., Well, R., 2017. Quantifying N_2 O reduction to N_2 based on N_2 O isotopocules – validation with independent methods (helium incubation and^{15} N gas flux method). Biogeosciences 14, 711–732. https://doi.org/10.5194/bg-14-711-2017

Liu, Yingrui, He, Y., Ren, S., Zhu, T., Liu, Yiwen, 2022. Selective Organic Carbon Enrichment Influences Nitrous Oxide Reduction by Denitrifiers: Electron Competition Insights. ACS EST Water 2, 1265–1275. https://doi.org/10.1021/acsestwater.2c00161

Mariotti, A., Germon, J.C., Hubert, P., Kaiser, P., Letolle, R., Tardieux, A., Tardieux, P., 1981. Experimental determination of nitrogen kinetic isotope fractionation: Some principles; illustration for the denitrification and nitrification processes. Plant Soil 62, 413–430. https://doi.org/10.1007/BF02374138

Mohn, J., Biasi, C., Bodé, S., Boeckx, P., Brewer, P.J., Eggleston, S., Geilmann, H., Guillevic, M., Kaiser, J., Kantnerová, K., Moossen, H., Müller, J., Nakagawa, M., Pearce, R., Von Rein, I., Steger, D., Toyoda, S., Wanek, W., Wexler, S.K., Yoshida, N., Yu, L., 2022. Isotopically characterised N_2 O reference materials for use as community standards. Rapid Commun. Mass Spectrom. 36, e9296. https://doi.org/10.1002/rcm.9296

Morley, N., Baggs, E.M., 2010. Carbon and oxygen controls on N2O and N2 production during nitrate reduction. Soil Biol. Biochem. 42, 1864–1871. https://doi.org/10.1016/j.soilbio.2010.07.008

Morley, N., Baggs, E.M., DÃ¶rsch, P., Bakken, L., 2008. Production of NO, N2O and N2 by extracted soil bacteria, regulation by NO2− and O2 concentrations: Production of NO, N2O and N2 by extracted soil bacteria. FEMS Microbiol. Ecol. 65, 102–112. https://doi.org/10.1111/j.1574-6941.2008.00495.x

Ostrom, N.E., Pitt, A., Sutka, R., Ostrom, P.H., Grandy, A.S., Huizinga, K.M., Robertson, G.P., 2007. Isotopologue effects during N_2 O reduction in soils and in pure cultures of denitrifiers. J. Geophys. Res. Biogeosciences 112, 2006JG000287. https://doi.org/10.1029/2006JG000287

Plouviez, M., Sperlich, P., Guieysse, B., Clough, T., Peethambaran, R., Wells, N., 2026. A novel laser-based spectroscopic method reveals the isotopic signatures of nitrous oxide produced by eukaryotic and prokaryotic phototrophs in darkness. Biogeosciences 23, 497–508. https://doi.org/10.5194/bg-23-497-2026

Pomowski, A., Zumft, W.G., Kroneck, P.M.H., Einsle, O., 2011. N2O binding at a [4Cu:2S] copper–sulphur cluster in nitrous oxide reductase. Nature 477, 234–237. https://doi.org/10.1038/nature10332

R Core Team, 2025. R: A Language and Environment for Statistical Computing.

Rees, A.P., Brown, I.J., Jayakumar, A., Lessin, G., Somerfield, P.J., Ward, B.B., 2021. Biological nitrous oxide consumption in oxygenated waters of the high latitude Atlantic Ocean. Commun. Earth Environ. 2, 36. https://doi.org/10.1038/s43247-021-00104-y

https://doi.org/10.5194/egusphere-2026-857
Preprint. Discussion started: 27 February 2026

Sperlich, P., Camin, F., Deufrains, K., Englund Michel, S., Hoheisel, A., Mohn, J., Schmidt, M., Tarasova, O., 2024. Measurement of the Stable Carbon Isotope Ratio in Atmospheric CH4 Using Laser Spectroscopy for CH4 Source Characterization, 1st ed. ed, IAEA TECDOC Series No Series. International Atomic Energy Agency, Vienna.

Strubbe, L., Keck, H., Magyar, P.M., Mohn, J., Joss, A., Froemelt, A., 2026. Activating specific N2O production pathways to understand emission dynamics in wastewater treatment. Water Res. 296, 125580. https://doi.org/10.1016/j.watres.2026.125580.

Suenaga, T., Riya, S., Hosomi, M., Terada, A., 2018. Biokinetic Characterization and Activities of N2O-Reducing Bacteria in Response to Various Oxygen Levels. Front. Microbiol. 9, 697. https://doi.org/10.3389/fmicb.2018.00697

Sutka, R.L., Ostrom, N.E., Ostrom, P.H., Breznak, J.A., Gandhi, H., Pitt, A.J., Li, F., 2006. Distinguishing Nitrous Oxide Production from Nitrification and Denitrification on the Basis of Isotopomer Abundances. Appl. Environ. Microbiol. 72, 638–644. https://doi.org/10.1128/AEM.72.1.638-644.2006

Tang, W., Jayakumar, A., Sun, X., Tracey, J.C., Carroll, J., Wallace, E., Lee, J.A., Nathan, L., Ward, B., 2022. Nitrous Oxide Consumption in Oxygenated and Anoxic Estuarine Waters. Geophys. Res. Lett. 49, e2022GL100657. https://doi.org/10.1029/2022GL100657

Tian, H., Pan, N., Thompson, R.L., Canadell, J.G., Suntharalingam, P., Regnier, P., Davidson, E.A., Prather, M., Ciais, P., Muntean, M., Pan, S., Winiwarter, W., Zaehle, S., Zhou, F., Jackson, R.B., Bange, H.W., Berthet, S., Bian, Z., Bianchi, D., Bouwman, A.F., Buitenhuis, E.T., Dutton, G., Hu, M., Ito, A., Jain, A.K., Jeltsch-Thömmes, A., Joos, F., Kou-Giesbrecht, S., Krummel, P.B., Lan, X., Landolfi, A., Lauerwald, R., Li, Y., Lu, C., Maavara, T., Manizza, M., Millet, D.B., Mühle, J., Patra, P.K., Peters, G.P., Qin, X., Raymond, P., Resplandy, L., Rosentreter, J.A., Shi, H., Sun, Q., Tonina, D., Tubiello, F.N., Van Der Werf, G.R., Vuichard, N., Wang, J., Wells, K.C., Western, L.M., Wilson, C., Yang, J., Yao, Y., You, Y., Zhu, Q., 2024. Global nitrous oxide budget (1980–2020). Earth Syst. Sci. Data 16, 2543–2604. https://doi.org/10.5194/essd-16-2543-2024

Toyoda, S., Yoshida, N., 1999. Determination of Nitrogen Isotopomers of Nitrous Oxide on a Modified Isotope Ratio Mass Spectrometer. Anal. Chem. 71, 4711–4718. https://doi.org/10.1021/ac9904563

Toyoda, S., Yoshida, N., Koba, K., 2015. Isotopocule analysis of biologically produced nitrous oxide in various environments. Mass Spectrom. Rev. 36, 135–160. https://doi.org/10.1002/mas.21459

Tumendelger, A., Toyoda, S., Yoshida, N., Shiomi, H., Kouno, R., 2016. Isotopocule characterization of N_2O dynamics during simulated wastewater treatment under oxic and anoxic conditions. Geochem. J. 50, 105–121. https://doi.org/10.2343/geochemj.2.0390

Werle, P., Mücke, R., Slemr, F., 1993. The limits of signal averaging in atmospheric trace-gas monitoring by tunable diode-laser absorption spectroscopy (TDLAS). Appl. Phys. B Photophysics Laser Chem. 57, 131–139. https://doi.org/10.1007/BF00425997

Wickham, H., 2016. ggplot2: elegant graphics for data analysis, Second edition. ed, Use R! Springer international publishing, Cham.

WMO, 2024. WMO Greenhouse Gas Bulletin No. 20 – 28 October 2024 The State of Greenhouse Gases in the Atmosphere Based on Global Observations through 2023, WMO Greenhouse Gas Bulletin. Geneva.

Wunderlin, P., Lehmann, M.F., Siegrist, H., Tuzson, B., Joss, A., Emmenegger, L., Mohn, J., 2013. Isotope Signatures of N_2 O in a Mixed Microbial Population System: Constraints on N_2 O Producing Pathways in Wastewater Treatment. Environ. Sci. Technol. 130118101927005. https://doi.org/10.1021/es303174x

Yu, L., Harris, E., Lewicka-Szczebak, D., Barthel, M., Blomberg, M.R.A., Harris, S.J., Johnson, M.S., Lehmann, M.F., Liisberg, J., Müller, C., Ostrom, N.E., Six, J., Toyoda, S., Yoshida, N., Mohn, J., 2020. What can we learn from N_2 O isotope data? – Analytics, processes and modelling. Rapid Commun. Mass Spectrom. 34, e8858. https://doi.org/10.1002/rcm.8858

Zhou, Y., Suenaga, T., Qi, C., Riya, S., Hosomi, M., Terada, A., 2021. Temperature and oxygen level determine N_2 O respiration activities of heterotrophic N_2 O-reducing bacteria: Biokinetic study. Biotechnol. Bioeng. 118, 1330–1341. https://doi.org/10.1002/bit.27654